2015 IEEE International Conference on Robotics and Automation (ICRA)
Washington State Convention Center
Seattle, Washington, May 26-30, 2015

A Kinematic Controller for Human-Robot Handshaking using Internal Motion Adaptation

Dimitrios Papageorgiou and Zoe Doulgeri

Abstract— **This work proposes a kinematic control method for human-robot handshake motions achieving fast motion synchronization given a preset internal robot handshake motion and a compliance level that reflects the robot's level of passiveness. The proposed method combines a non-linear dynamic system having an attractive limit cycle with an admittance controller and an adaptation mechanism so that interaction forces are minimized and a consensus oscillation is achieved between the engaging participants. The proposed method is validated by experimenting with a KUKA LWR4+ 7dof arm under various scenarios.**

I. INTRODUCTION

Handshaking is a common physical interaction utilized when humans are introduced to one another for the first time, or in greeting each other. Socially it symbolizes acceptance and respect for the other person and may lead to future cooperation and coexistence. To achieve a successful handshaking, both participants have to be synchronized. It is believed that this synchronization of the embodied rhythms, establishes an accepted relationship and a feeling of safety[1].

The handshake procedure could be divided in two phases: the approaching motion and the shake motion. Previous works have discussed solutions for each of the phases above, but synchronization during the shake-motion is a more discussed issue. For the first phase an approaching motion is proposed under the assumption that the human is always the requester and the robot is the respondent [1], [2], [3]. The approach in [1], [2], [3] is heavily based on vision in order to acquire online the human arm configuration trajectory and produce its mirror with a delay for the robot.

For the shake motion phase, it is generally accepted that there is a passive and an active participant. Most of the works assume the passiveness of the robot and propose a solution in which the robot synchronizes with the human, based on the interaction force. In particular, in [3], an impedance controller is utilized and the synchronization is achieved via the adaptation of the control parameters. A synchronization technique using neural oscillators in the robot joints is proposed in [4] adapting the amplitude and the frequency of the shake motion according to the interaction force. The method involves a multitude of parameters in the general case requiring extensive tuning to produce a natural result but can deal with various levels of passiveness. Another method proposed in [5] uses the interaction force measurements to identify human internal motion and produce dynamically an attractive robot motion trajectory but it is not validated with experimental results. Orbit attractors have also been used in motion transfer applications [6].

Taking another perspective, [7] utilizes the interaction force to classify the human intention as a passive or active based on a second order human impedance model estimation. The impedance parameters of an admittance controller and the amplitude and frequency of active oscillation are changed according to the result of the classification. Although there may be a great advantage to know the human intention, the classifier needs to be trained based on a big dataset.

Another method is based on the switching between a predictive controller which is used to generate an active shake motion and a reactive controller which provides compliant abilities [8]. This method switches from the reactive to the predictive controller whenever a steady state oscillation is achieved. Practically, determining the steady-state phase may be difficult and strict thresholds may result in frequently switching between the controllers if the oscillation is not harmonic.

In this work, we propose a handshake kinematic controller, which is based on an adaptable internal motion generator producing a consensus oscillation between a human and a robot that may take any role regarding the level of passiveness. The proposed method is described in Section II. An experimental study under various scenarios is described in Section III. Conclusions are drawn in Section IV.

II. PROPOSED METHOD

The main idea of the proposed method is based on the assumption that each participant has an internal motion rhythm generator for handshaking, but is also willing to be compliant to the external forces in order to synchronize. Hence the robot should behave accordingly. The main problem in handshaking is to achieve a steady harmonic motion between the two hands, minimizing the interaction contact forces.

The proposed scheme for robot handshaking control is shown in Fig.1. It contains an adaptable internal motion generator, which is implemented as a 2^{nd} order non-linear dynamical system with a limit cycle attractor, reflecting a harmonic oscillation of specific characteristics. The attractiveness of the limit cycle means that when disturbed, the system trajectory would eventually return to the oscillation.

This research is co-financed by the EU-ESF and Greek national funds through the operational program "Education and Lifelong Learning" of the National Strategic Reference Framework (NSRF) - Research Funding Program ARISTEIA I

The authors are with the Department of Electrical and Computer Engineering, Aristotle University of Thessaloniki, 54124 Thessaloniki, Greece. emails: dimpapag@eng.auth.gr, doulgeri@eng.auth.gr

During handshaking, the robot experiences an interaction force which is assumed to be available for measurement (e.g. via the robot joint torque sensors). The magnitude of this force is an indication of the level of synchronization between the two hands. In order to be compliant to this force, the proposed scheme includes an admittance model which is implemented as a 2nd order linear mass-damper-spring dynamical system:

$$M_d\ddot{d}(t) + B_d\dot{d}(t) + K_d d(t) = F \tag{1}$$

where $F \in \Re^3$ is the measured contact force, $M_d, B_d, K_d \in \Re^{3\times3}$ are the desired impedance parameters. The values of those parameters may be selected from human impedance measured values [9], [10], [11]. The choice of a specific impedance reflects the level of desired compliance of the robot to an external force. The superposition of the internal motion generator output p_r, $\dot{p}_r \in \Re^3$ and the output of the admittance model d, $\dot{d} \in \Re^3$ is utilized to adapt the internal motion generator parameters via a Direct Least Square (DLS) fitting of ellipses in state space (Fig.1). The latter is performed only in the direction of the gravity field, as we assume that this is the main direction of a handshake motion. For this reason the z-coordinate of the desired trajectory $p_d \in \Re^3$ and velocity $\dot{p}_d \in \Re^3$ are extracted as follows:

$$\begin{aligned} z_d &= p_d^T e_z \\ \dot{z}_d &= \dot{p}_d^T e_z \end{aligned} \tag{2}$$

where $e_z = [0\ 0\ 1]^T \in \Re^3$ is the unit vector in the direction of the shake motion, $p_d = p_r + d$ and $\dot{p}_d = \dot{p}_r + \dot{d}$.

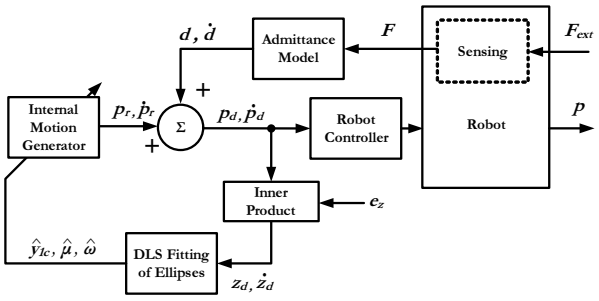

Fig. 1. General Diagram of proposed method

A detailed description of the proposed method follows.

A. Internal motion generator

In this work, a classic Hopf oscillator is utilized, which exhibits an attractive circular limit cycle:

$$\begin{aligned} \dot{y_1} &= \gamma(\mu - ((y_1 - y_{1c})^2 + y_2^2))(y_1 - y_{1c}) - \omega y_2 \\ \dot{y_2} &= \gamma(\mu - ((y_1 - y_{1c})^2 + y_2^2))y_2 + \omega(y_1 - y_{1c}) \end{aligned} \tag{3}$$

where y_1 and y_2 are the state variables,γ a parameter affecting the convergence in the limit cycle, ω the angular frequency of the oscillation and $\mu = r^2$, where r is the radius of the circle and $y_c = [y_{1c}\ 0]$ is its center. The attractiveness of the limit cycle can be proved by considering:

$$V(y_1, y_2) = \frac{1}{2}(\mu - (y_1 - y_{1c})^2 + y_2^2)^2 \tag{4}$$

which is $V(y_1, y_2) = 0$, for every y_1, y_2 belonging to the circle $((y_1 - y_{1c})^2 + y_2^2) = \mu$ and noticing that its derivation yields:

$$\dot{V} = -2\gamma(\mu - ((y_1 - y_{1c})^2 + y_2^2))^2((y_1 - y_{1c})^2 + y_2^2) \leq 0 \tag{5}$$

Let $x = [x_1\ x_2]^T$ be the internal motion generator state, where $x_1, x_2 \in \Re$ are the shake motion position and velocity along the handshake direction respectively. We can convert the Hopf oscillator limit cycle $(y_1(t) - y_{1c})^2 + y_2^2 = \mu$ to the x-space by setting $x_1 = y_1$ and $x_2 = \dot{y}_1$ in the first equation of (3). This implies $x_2 = -\omega y_2$ when the state is on the limit cycle; substituting y_1 and y_2 in the limit cycle equation yields an ellipse in the x-plane:

$$\frac{(x_1 - y_{1c})^2}{r^2} + \frac{x_2^2}{\omega^2 r^2} = 1 \tag{6}$$

The following direct mapping from y-space to x-space

$$\begin{aligned} x_1 &= y_1 \\ x_2 &= \gamma(\mu - ((y_1 - y_{1c})^2 + y_2^2))(y_1 - y_{1c}) - \omega y_2 \end{aligned} \tag{7}$$

is utilized to produce the output of the adaptable internal motion generator, which is consequently transformed to a reference position trajectory for the robot's end-effector by:

$$p_r = x_1 e_z\ ,\ \dot{p}_r = x_2 e_z \tag{8}$$

The inverse mapping (from x-space to y-space) is required when we need to solve system (3), given an initial state $x(t_0) = [x_{10}\ \ x_{20}]^T$; thus, $y(t_0) = [y_{10}\ \ y_{20}]$ has to be computed. As the inverse mapping is the solution of quadratic equation in y_{20}, a feasible $y_{20} \in \Re$ exists under the following condition:

$$(g(\delta_x, \omega, \mu, \gamma) - x_2)\delta_x > 0 \tag{9}$$

where $\delta_x = x_1 - y_{1c}$ and

$$g(\delta_x, \omega, \mu, \gamma) = \frac{\omega^2}{4\gamma}\frac{1}{\delta_x} - \gamma\delta_x^3 + \gamma\mu\delta_x \tag{10}$$

Limit cycle parameters ω, μ, γ and y_{1c} should satisfy condition (9) for a feasible solution to exist. In this work, the feasibility of the inverse mapping is achieved by appropriately selecting γ, since the rest of the oscillation parameters are given by the output of the internal motion adaptation.

B. Internal motion adaptation

The adaptation is done in every sampling interval T_a. At the $k-$th sample:

(i) Estimates of the limit cycle parameters ($\hat{y}_{1c}$, $\hat{\mu}$ and $\hat{\omega}$) are calculated based on the n previous samples of the desired trajectory $z_{d(k-i)}$ and $\dot{z}_{d(k-i)}$, where $i = 0...n-1$ (2) (Fig.1) (see Remark 1, below).

(ii) Utilizing parameter estimates of step (i) and the current internal motion state x_{1k}, x_{2k}, (7) is resolved to produce an initial y-state y_{10}, y_{20} state, required in the next

step. This guarantees the continuity in the x variables (see Remark 2, below).

(iii) Using initial y_{10}, y_{20} state, system (3) is integrated with Runge-Kutta with fixed step equal to the control cycle T_s, in order to produce the desired trajectory.

(iv) the handshake trajectory is calculated from (7) and (8).

Remark 1: The limit cycle parameter estimation in step (i) is achieved by utilizing the ellipse-specific Direct Least Square fitting method [12]. Specifically, by utilizing the equation:

$$az_d^2 + b\dot{z}_d^2 + cz_d + d = 0 \tag{11}$$

and denoting $\boldsymbol{\theta} = [a\ b\ c\ d]^T$, the DLS method produces its estimate $\hat{\boldsymbol{\theta}}$. Based on the parameter vector $\hat{\boldsymbol{\theta}}$, the estimated center $\hat{y}_{1c}$, the square of the amplitude $\hat{\mu}$ and the angular frequency $\hat{\omega}$ of the oscillation are calculated.

Remark 2: Step (ii) is utilized to guarantee the velocity continuity in the x-plane. As it is clear from the direct mapping (7), when the parameter estimates of the limit cycle change there is a discontinuity in the x-plane for a continuous y-state. Using the inverse mapping, for the current value of x, ensures x-continuity at every change of the ellipse parameter estimates. Out of the two solutions derived from the inverse mapping, the closer to the current y value is selected.

C. Illustrative example of internal motion adaptation

In order to demonstrate the performance of the ellipse fitting method, we consider 2 harmonic oscillations. The first is centered at $y_{1c} = 5$, of amplitude $r = 1$ and frequency of $f = 2Hz$ and the second is centered at $y_{1c} = 5.2$, has an amplitude of $r = 0.8$ and a frequency of $f = 5Hz$. A noise signal of 0.01 maximum amplitude, produced by a uniform distribution generator, was added to both oscillations. Then, 10 samples were taken from each ellipse, equally distributed in one period for the first oscillation and in one quarter of the period for the second. The fitting of ellipses was consequently performed for each dataset separately. The normalized error e_p is depicted in Fig.2 for each case.

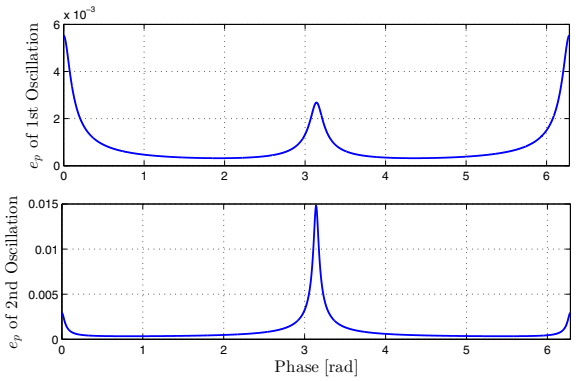

Fig. 2. Normilized error of ellipse estimations

When samples from the whole period are used, the estimation error (maximum 0.55%) is lower than the error achieved (maximum 1.47%) when samples are taken from only a quarter of the period as shown in Fig.2; nevertheless, the latter may still be considered satisfactory for the current application.

Subsequently, we have utilized the previous estimated ellipses to demonstrate the continuity preservation mechanism for the x-state, utilized in step (ii). We specify the initial value of x at $x(0) = [3.5\ \ 0]$ and the transition from the first to the second limit cycle at time $t_1 = 0.5s$. Fig.3 and 5 show the solution trajectories of (3) in the x and y state plane respectively, while Fig.4 shows $x_1(t)$, $x_2(t)$ as well as $y_2(t)$. Notice the discontinuity of y_2 at the parameter change time instant t_1 which is also clear from the state plane solution (Fig.5), while x-values remain continuous. As shown in Fig.3, the x-state initially converges to the first limit cycle since $x(0)$ does not belong to it; then, the transition at $t_1 = 0.5s$ occurs before the completion of one period and is followed by the convergence of the x-state to the second limit cycle Fig.3.

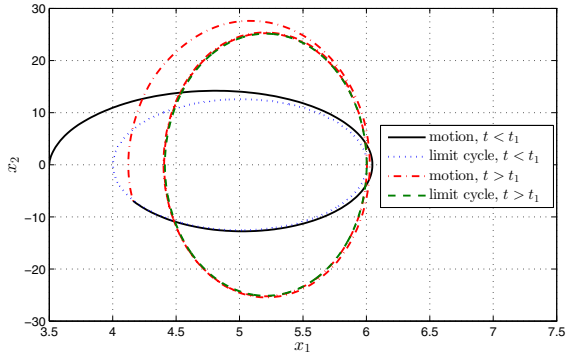

Fig. 3. Internal motion generator output in x-space

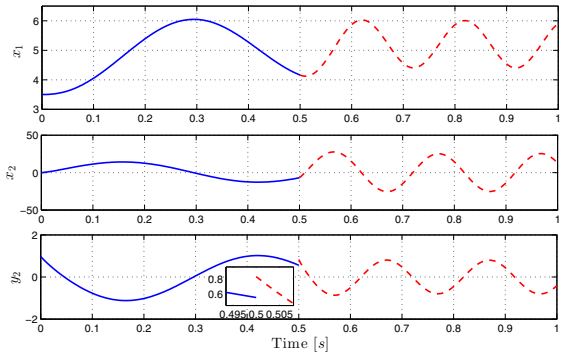

Fig. 4. Internal motion generator output and y_2 in time

III. Experiments

Handshake experiments are performed between a human and the KUKA LWR4+ 7dof manipulator (Fig.6). KUKA KRC2 controller is connected, via ethernet, to an external computer, utilizing a point-to-point dedicated network. The proposed method is implemented in C++ utilizing the FRI library, and is executed on an external computer with a

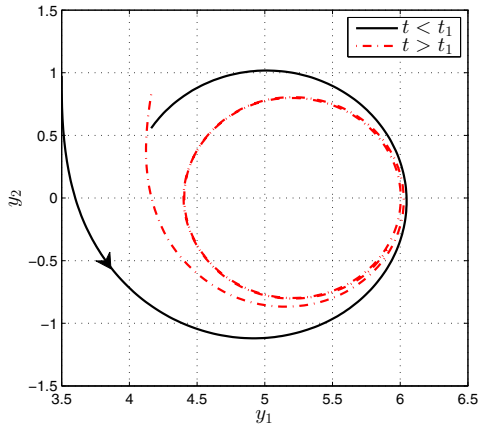

Fig. 5. y-state during motion generation.

control cycle of $T_s = 2ms$. The hand-shake procedure initially involves reaching a starting end-effector position, ($p_0 = [-0.54 \ \ -0.33 \ \ 0.22]m$) appropriate for handshake engagement by utilizing the prescribed performance controller (PPC) proposed in [13] . The shake motion is triggered when the human initial force in the handshake direction exceeds a prespecified threshold ($7N$). If the applied force is upwards, the starting end-effector position is taken as the lower peak of the intended oscillation, and vice versa. Triggering could also be done by tactile sensing if available. Notice that the admittance model is active since the beginning of the robot motion for all 3 dimensions. Thus, after triggering, the lower loop in Fig.1 comes into play. The robot's natural internal motion is set to the following harmonic oscillation: $f = 1.5Hz$ and $r = 0.04m$. The adaptation interval is set to $T_a = 0.132s$ and $n = 7$ previous samples are taken for the ellipse estimation. In order to filter the estimate spikes of $\hat{y}_{1c}$, $\hat{\mu}$ and $\hat{\omega}$ that appeared during the implementation, a moving average of $m = 3$ coefficients is used for every estimated ellipse parameter.

The proposed method achieves a consensus oscillation between the robot and the human internal motion according to the admittance parameter values in the robot controller. The admittance, which reflects the degree of the robot's "passiveness", for the experiments presented in this work, corresponds first, a relatively passive robot ($K_d = 200I_3 N/m$), second a relatively active robot ($K_d = 1200I_3 N/m$), with I_3 denoting the identity matrix of dimension 3 and last, the case of a non-homogeneous stiffness ($K_d = diag([25\ 25\ 200])N/m$). The latter reflects the willingness to be extremely compliant to any lateral forces and hence shift laterally the handshake oscillation. All admittance model parameters utilized in the experiments are shown in Table I; damping was carefully chosen to yield a critical damped response.

The first experimental set-up involves the relatively passive robot (set 1) and the cases of a passive and an active human. Notice that even for the case of a passive human the initial triggering force is needed. The active human scenario

TABLE I

EXPERIMENTAL ADMITTANCE MODEL PARAMETER SETS

Set	$M_d[Ns^2/m]$	$B_d[Ns/m]$	$K_d[N/m]$
1	$4I_3$	$60I_3$	$200I_3$
2	$4I_3$	$140I_3$	$1200I_3$
3	$4I_3$	$60I_3$	$diag([25\ 25\ 200])$

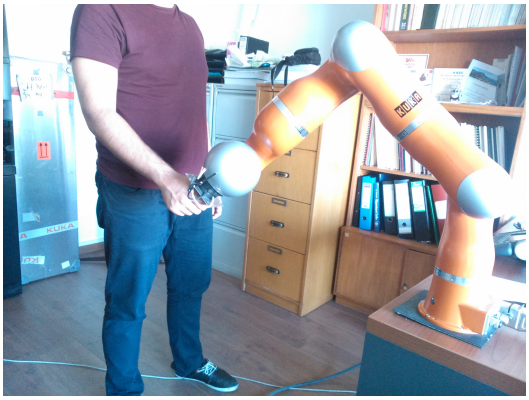

Fig. 6. Experimenting with a KUKA LWR4+. Starting end-effector position.

involves a lower frequency in the human internal oscillation to that of the robot. The second experimental set-up involves the relatively active robot (set 2) with a passive human. The third experimental set-up of non-homogenenous stiffness (set 3) involves an active human who in addition tries to impose a lateral shift in the hand-shake position.

Fig.7 shows the z-coordinate of the end-effector position and interaction force (p_z and F_z) and figures 8 & 9 show the end-effector position and force in the lateral directions for the first and second experimental set-ups. Notice how a stiff robot (relatively active robot, dashed-dotted line in Fig.7), combined with a passive human, results in an oscillation close to the internal robot motion. In case of the low stiffness robot (relatively passive robot) the initial handshake triggering force of the passive human ($31N$ at maximum, dashed line in Fig.7) affects the oscillation due to adaptation; thus the consensus oscillation in the latter case (dashed line in Fig.7) differs from the internal robot motion. Specifically, the center of oscillation, amplitude and frequency are approximately $0.28m$, $0.065m$ and $1.2Hz$ respectively. In general, the rate and magnitude of the triggering force affects the degree of changes of the internal robot motion. In the case of the active human scenario, Fig.7 (solid line) shows how the proposed method synchronizes with the lower frequency of the human's oscillation reducing the interaction forces in less than a period. The lateral position and forces in all the previous scenarios (Fig.8 & 9) show how the robot stays close to the starting position particularly in the active robot set-up.

For the third experimental set-up, Fig.10 shows the z-coordinate of the end-effector position and interaction force (p_z and F_z) and figures 11 & 12 show the end-effector position and force in the lateral directions. Notice the lateral

shift of the oscillation in the y-direction complying to the respective human force (Fig.12). Due to the very low stiffness in the y direction the force drops after the lateral transition transients; taking the steady state values of the displacement and the force in the y-direction we get approximately $27N/m$ which is close to the specified stiffness of $25N/m$. Further notice the fast adaptation of the handshake oscillation (Fig.10) with interaction forces minimized within $2s$ which is even before the completion of the lateral shift.

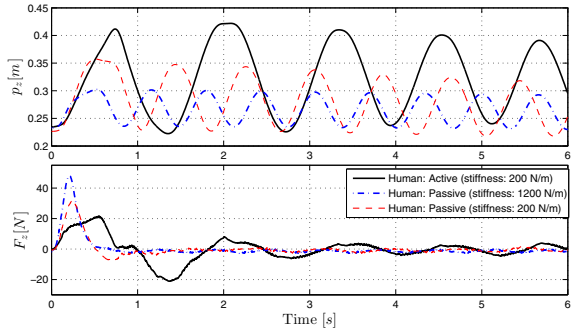

Fig. 7. End-effector position (p_z) and interaction forces (F_z), in first and second experimental setups.

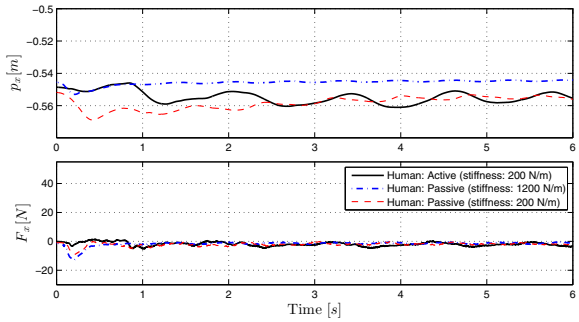

Fig. 8. End-effector position (p_x) and interaction forces (F_x), in first and second experimental setups.

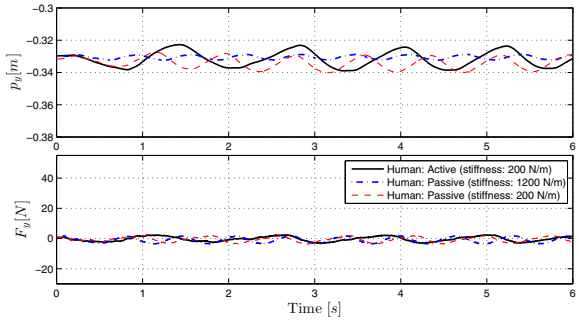

Fig. 9. End-effector position (p_y) and interaction forces (F_y), in first and second experimental setups.

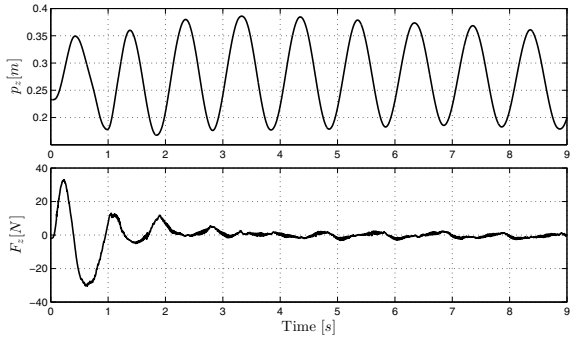

Fig. 10. End-effector position (p_z) and interaction forces (F_z), in third experimental setup.

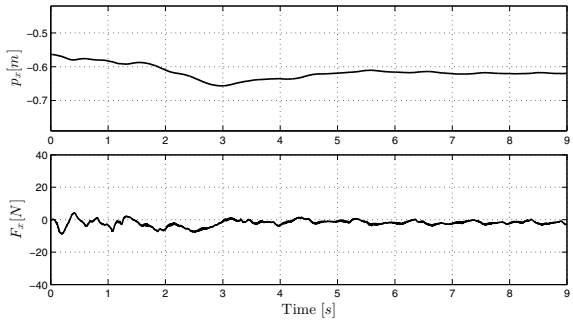

Fig. 11. End-effector position (p_x) and interaction forces (F_x), in third experimental setup.

IV. CONCLUSIONS

This work proposes a kinematic control method for human-robot handshake motions utilizing an attractive limit cycle adaptation mechanism in order to achieve a consensus oscillation by fast minimizing interaction forces. The proposed method produces a continuous trajectory for the robot's end-effector, which is validated by experimenting with a KUKA LWR4+ 7dof arm under various scenarios. Experimental results show fast achievement of a synchronized motion. Future work includes psychological evaluation of the robot handshake, as well as extending this methodology for teaching robots, via physical human-robot interaction.

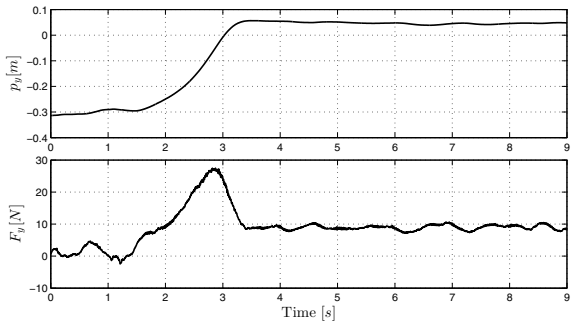

Fig. 12. End-effector position (p_y) and interaction forces (F_y), in third experimental setup.

REFERENCES

[1] M. Jindai, T. Watanabe, S. Shibata, and T. Yamamoto, "Development of a handshake robot system for embodied interaction with humans," in *Robot and Human Interactive Communication, 2006. ROMAN 2006. The 15th IEEE International Symposium on*, 2006.

[2] M. Jindai and T. Watanabe, "A handshake robot system based on a shake-motion leading model," in *Intelligent Robots and Systems, 2008. IROS 2008. IEEE/RSJ International Conference on*, 2008.

[3] Y. Yamato, M. Jindai, and T. Watanabe, "Development of a shake-motion leading model for human-robot handshaking," in *SICE Annual Conference, 2008*, 2008.

[4] T. Kasuga and M. Hashimoto, "Human-robot handshaking using neural oscillators," in *Robotics and Automation, 2005. ICRA 2005. Proceedings of the 2005 IEEE International Conference on*, 2005.

[5] T. Sato, M. Hashimoto, and M. Tsukahara, "Synchronization based control using online design of dynamics and its application to human-robot interaction," in *Robotics and Biomimetics, 2007. ROBIO 2007. IEEE International Conference on*, 2007.

[6] M. Okada and M. Watanabe, "Pseudo-reference for motion transfer based on autonomous control system with an orbit attractor," in *Intelligent Robots and Systems (IROS), 2010 IEEE/RSJ International Conference on*, Oct 2010, pp. 1297–1302.

[7] Z. Wang, A. Peer, and M. Buss, "An hmm approach to realistic haptic human-robot interaction," in *EuroHaptics conference, 2009 and Symposium on Haptic Interfaces for Virtual Environment and Teleoperator Systems. World Haptics 2009. Third Joint*, 2009.

[8] Y. Chua, K.-P. Tee, and R. Yan, "Human-robot motion synchronization using reactive and predictive controllers," in *Robotics and Biomimetics (ROBIO), 2010 IEEE International Conference on*, 2010.

[9] T. Tsuji, P. G. Morasso, K. Goto, , and K. Ito, "Human hand impedance characteristics during maintained posture," *Biological Cybernetics*, vol. 72, no. 6, pp. 475–485, 1995.

[10] P. K. Artemiadis, P. T. Katsiaris, M. V. Liarokapis, , and K. J. Kyriakopoulos, "Human arm impedance: Characterization and modeling in 3d space," in *IEEE/RSJ International Conference on Intelligent Robots and Systems (IROS)*, 2010, pp. 3103 – 3108.

[11] a. D. Y. L. Hyun Soo Woo, "Exploitation of the impedance and characteristics of the human arm in the design of haptic interfaces," *IEEE Transactions on Industrial Electronics*, vol. 58, no. 8, pp. 3221–3233, 2011.

[12] A. Fitzgibbon, M. Pilu, and R. Fisher, "Direct least square fitting of ellipses," *Pattern Analysis and Machine Intelligence, IEEE Transactions on*, 1999.

[13] A. Atawnih, D. Papageorgiou, and Z. Doulgeri, "Reaching for redundant arms with human-like motion and compliance properties," *Robotics and Autonomous Systems*, vol. 62, no. 12, pp. 1731 – 1741, 2014.